1997MNRAS.286.1012F

Mon. Not. R. Astron. Soc. **286,** 1012–1022 (1997)

The luminosity function of the globular cluster NGC 6752 with the *Hubble Space Telescope*: evidence of mass segregation

F. R. Ferraro,[1★] E. Carretta,[1★] A. Bragaglia,[1★] A. Renzini[2,3★] and S. Ortolani[4★]

[1] *Osservatorio Astronomico, via Zamboni 33, I-40126 Bologna, Italy*
[2] *European Southern Observatory, D-85748 Garching bei München, Germany*
[3] *Università di Bologna, Dipartimento di Astronomia, via Zamboni 33, I-40126 Bologna, Italy*
[4] *Università di Padova, Dipartimento di Astronomia, vicolo Osservatorio 5, I-35100 Padova, Italy*

Accepted 1996 December 14. Received 1996 November 12; in original form 1996 September 25

ABSTRACT

We present the luminosity function (LF) for the lower main sequence of the Galactic globular cluster NGC 6752, as obtained from *Hubble Space Telescope* (*HST*) observations centred 2 arcmin from the cluster centre. We present data in the F814W and F555W filters. Our LF reaches down to $M_I = 11$ or, translated to a mass function, to $M \simeq 0.12$ M$_\odot$. The LF reaches a maximum between $M_I = 8.5$ and 9, and shows no indication of an increase towards lower luminosities/masses; this is at variance with some ground-based observations, but is similar to all other *HST*-based LFs. There is a clear indication of mass segregation since the relative numbers of bright/faint stars differ from that found in ground-based observations and in other clusters analysed with the *HST*.

Key words: stars: fundamental parameters – Hertzsprung–Russell (HR) diagram – stars: low-mass, brown dwarfs – globular clusters: individual: NGC 6752 – Galaxy: stellar content.

1 INTRODUCTION

The luminosity function (LF) of a globular cluster (GC) is an important source of information for a wide set of astrophysical problems. These include (1) stellar evolution (for the part of the LF at luminosities brighter than the main-sequence turn-off (MSTO); (2) star formation, via the mass function (MF) that can be derived from the LF below the MSTO, and finally (3) information on the cluster dynamical state and evolution, from the radial dependence of the LF signalling mass segregation effects within the clusters.

The data used in this paper do not include enough evolved stars, hence point (1) above is not discussed any further. Concerning point (2), the interesting quantity is of course the initial mass function (IMF). There is, however, a long way to go from the cluster LF to the IMF. Translating an LF into an MF requires the use of a mass–luminosity (M–L) relation. Moreover, the process will provide the present-day mass function (PDMF) of the cluster (essentially limited to low-mass stars with $M \lesssim 0.85$ M$_\odot$), which may differ significantly from the IMF because of preferential escapes of lower-mass stars during the dynamical evolution of the cluster.

The theoretical M–L relation for low-mass stars is presently subject to major uncertainties, including the lack of an empirical test, especially at the low metallicity of most Galactic globular clusters. The uncertainties come from the complications brought about by the unique temperature–density conditions prevailing in these stars, which affect the equation of state and the opacity. Moreover, colour–temperature transformation and bolometric corrections are especially uncertain towards the lower end of the main sequence (MS), where stars belong to the spectral type M, and the spectral energy distribution is dominated by molecular features.

Notwithstanding these limitations, the astrophysical importance of the IMF makes the study of the LF of globular clusters an essential step, especially in connection with the question of a possible baryonic contribution to dark matter. Crowding has further limited ground-based efforts at determining the clusters' LF. Much of this limitation has now been removed by the *HST*, which allows exploration of the cluster LF both at very faint magnitudes and close to the cluster centre. Several globular cluster LFs derived from *HST* data are now available, namely for NGC 6397 (Paresce, De Marchi & Romaniello 1995; Cool, Piotto & King

★E-mail: ferraro@astbo3.bo.astro.it (FRF); carretta@astbo3.bo.astro.it (EC); angela@astbo3.bo.astro.it (AB); arenzini@eso.org (AR); ortolani@astrpd.pd.astro.it (SO)

© 1997 RAS

Downloaded from https://academic.oup.com/mnras/article/286/4/1012/978305 by guest on 21 August 2022

© Royal Astronomical Society • Provided by the NASA Astrophysics Data System

1997MNRAS.286.1012F

1996), ω Cen (Elson et al. 1995), 47 Tuc (De Marchi & Paresce 1995b; Santiago, Elson & Gilmore 1996), and M15 (De Marchi & Paresce 1995a; Piotto, Cool & King 1996). Evidence for mass segregation within the cluster has been presented for NGC 6397, comparing the LF from Faint Object Camera (FOC) and Wide Field Planetary Camera 2 (WFPC2) data, respectively 7 arcsec and 4.6 arcmin from the centre (King, Sosin & Cool 1995), for 47 Tuc observed at the centre and ~12 core radii away (Anderson & King 1996), and for M15 (De Marchi & Paresce 1996).

NGC 6752 is another very close cluster for which *HST* data have been obtained (Shara et al 1995; Rubenstein & Baylin 1997), but the exposures are rather shallow and refer to the most central portion of the cluster. Here we present results for NGC 6752, based on very deep *HST* exposures (Renzini et al. 1996). In Section 2 we present our data and the reduction procedure, while in Section 3 we derive the LF and compare it to other LFs, discussing mass segregation. In Section 4 we attempt to derive the MF by using several theoretical M–L relations as available in the literature. Our main conclusions are finally summarized in Section 5.

2 DATA ACQUISITION AND REDUCTION

NGC 6752 was observed by the *HST* with the WFPC2 on 1995 March 30 and April 1, in the F336W, F439W, F555W and F814W filters as part of a project aimed at deriving an accurate distance for this cluster (hence its age) from the cluster white dwarf cooling sequence (Renzini et al. 1996). Here only data for the F814W ('*I*') and F555W ('*V*') filters will be examined, as they are the best suited to study the lower MS. Correspondingly, the data set consists of 5×1200 s exposures in *V* and 7×1000 s exposures in *I*.

The field is centred about 2 arcmin due south-east of the cluster centre ($\alpha_{2000} = 19^h\ 11^m\ 01\overset{s}{.}2$, $\delta_{2000} = -60°\ 01'\ 14''$), corresponding to ~12 core radii, or about one half-light radius. This assumes a core radius of $r_c = 10.5$ arcsec and a half-light radius $r_h = 115$ arcsec (Trager, Djorgorski & King, 1993). Fig. 1 shows the limits of the WFPC2 field of view, which covers distances from about 1 to 4 arcmin from the cluster centre (corresponding to 6–24 r_c, or 0.5–2 r_h).

Of the four chips forming the WFPC2, we present first the results for WF3, which is at an intermediate distance from the cluster centre, then make comparisons with the other chips. The WF3 images are the best compromise between fairly low crowding (relative e.g. to WF2, the worse case) and a lack of strongly blooming stars (which can affect the background, hence star detectability) on one hand, and the number of stars (hence their statistical significance) on the other hand. The LF has also been constructed for the PC, the least crowded portion of WF2, and for the portion of WF4 farther away from the cluster centre. The selected regions are shown in Fig. 1 as dotted areas.

Because of the long *HST* exposures, stars in the upper MS [$V \lesssim 20$, about 3 mag below the turn-off (TO)] are saturated. In order to extend the colour–magnitude diagram (CMD) and the LF to brighter magnitudes, we have complemented the *HST* data with ground-based *V* and *I* observations with the European Southern Observatory New Technology Telescope (ESO NTT), obtained for the same field covered by the *HST*, and with very good seeing ($\lesssim 0.55$ arcsec). The telescope was equipped with the SUSI direct camera, mounting the Tektronix CCD n. 25, giving a field of view of 2.1×2.1 arcmin^2, with a pixel size of 0.13 arsec. The exposure time was 240 s in both *V* and *I*. Correction for incompleteness was derived in the usual way, with artificial star tests repeated three times per mag bin; in the following discussion we will consider only those bins for which the correction is less than 50 per cent. An indirect, but strong, proof of the validity of the corrections so computed comes from Fig. 6a (see below): the NTT and WF3 LFs, after incompleteness corrections, appear very similar in the magnitude range they have in common, i.e. for the faintest bins in the case of NTT, but for the brightest and more reliable ones for WF3. Finally, stars in the two data sets were cross-identified, and the ground-based magnitudes were homogenized to the *HST* system.

2.1 *HST* and NTT data analysis

The data were processed through the standard *HST* pipeline for bias, dark and flat-field corrections, while all subsequent reductions were carried out using MIDAS routines and the ROMAFOT (Buonanno et al. 1983) package for crowded fields, in a version specifically adapted to handle *HST* data (Buonanno & Iannicola 1988). The five *V* frames and the seven *I* frames were aligned, cosmic ray events were removed, and finally the *V* and *I* frames were averaged, thus obtaining a median image.

The star search was then performed on the median *I* image, since it reaches fainter stars (given the colours of the lower main sequence). The standard routine for object detection was set for a 5σ threshold above local background level. The point-spread function (PSF) was obtained from

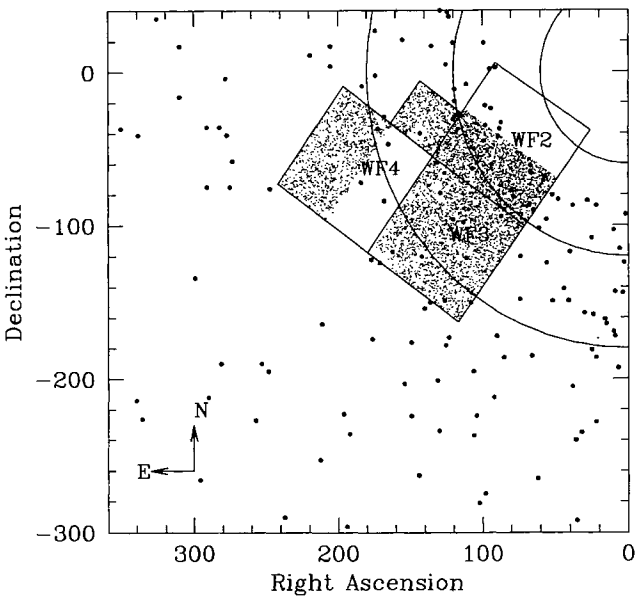

Figure 1. Position of our field of view, superimposed on the Buonanno et al. (1989) data, shown as filled circles. The dotted regions show which part of the chips was used in deriving the cluster LF. East and north are indicated by arrows, and the scale is in arcsec, both in right ascension and declination. The three circles are drawn at 60, 120 and 180 arcsec from the centre.

© Royal Astronomical Society • Provided by the NASA Astrophysics Data System

Downloaded from https://academic.oup.com/mnras/article/286/4/1012/978305 by guest on 21 August 2022

1997MNRAS.286.1012F

the brightest, unsaturated, isolated stars, and compared with artificial stars synthesized by the TINY TIM software package (Krist 1994). It has then been modelled by a Moffat (1969) function in the central part of the profile, plus a numerical map of the residuals for a better rendition of the wings.

All candidate stars were fitted in the median I and V frames using PSF profile fitting, thus producing a preliminary CMD. Objects falling far from the MS or/and having the goodness-of-fit parameter (χ) 5σ away from the mean value ($<\chi>$) computed on all objects were examined by eye: most were defects (i.e. remaining cosmic ray events; enhancements over the background resulting from the crossing of diffraction patterns of nearby stars; hot pixels, etc.) and were eliminated from the list. The final catalogue for the WF3 field contains about 2500 stars.

These 2500 objects have been re-measured separately on each single frame, and the magnitudes presented here are the average of up to five measurements in V and up to seven measurements in I (disregarding those measurements compromised by cosmic ray events). The calibration to Johnson V and I was carried out following the Holtzman et al. (1995) recipes. The aperture corrections to 0.5 arcsec were derived for all fields, magnitudes were referred to 1 s exposure time, and equation (8) and table 7 of Holtzman et al. (1995) have been used to derive the final magnitudes. The ground-based data have been processed with DAOPHOT II standard procedure (Stetson 1987, 1992), and corrected for completeness using the artificial stars routine within DAOPHOT.

Fig. 2 shows the resulting composite CMD for stars within the WF3 field. The MS of the cluster is very narrow and well defined down to $V \lesssim 26$. An inflexion point is present at $V \lesssim 22.5$ $V-I \lesssim 1.65$, and another at $V \lesssim 25$, $V-I \lesssim 2$, a distinct feature in all deep globular cluster CMDs obtained with the *HST* (e.g. Cool et al. 1996). As shown in Figs 2 and 3, a sequence of binary candidates is present, brighter and redder than the main sequence. The presence of binaries is also corroborated by the findings of Rubenstein & Baylin (1997) who observed the very central part of NGC 6752 and found a large fraction of binary systems (fraction decreasing from the centre outwards). We plan to present a detailed analysis of the binary sequence in a forthcoming paper. On the left side of the CMD, some white dwarfs (WD) are clearly visible; we do not expand on them, since complete CMDs for the WD component, involving all four filters, will be presented elsewhere (Bragaglia et al., in preparation). We only note in passing that nine out of the 14 WDs found in an independent search on the F439W frames (better suited to search for blue objects) were also recovered in the I frames. A few objects lying between the two sequences were eliminated as being the result of contamination from nearby stars.

The number of field stars and faint galaxies expected in our field was deduced from table 1 in Bahcall, Guhathakurta & Schneider (1990), scaling to the WF3 area. The number of stars is negligible at the high Galactic latitude of NGC 6752, and galaxies become noticeable only fainter than about $I = 22$ (about 10 with $I = 22$–23 are expected in our field of view). This small field contamination does not affect the LF determination (see next section), since we counted only stars in proximity to the MS.

Stars within the PC field and the selected portions of the WF2 and WF4 fields were measured in exactly the same way, on both the *HST* and the NTT frames. Fig. 3 shows the resulting CMDs, which are of course very similar to those obtained for the WF3 field. A comparison of the four CMDs allows an eye estimate of the effect of the different crowding conditions.

In order to estimate the completeness of the star sample as a function of magnitude we have followed the procedure described in Ferraro et al. (1990). A set of stars at different magnitude levels have been simulated using the TINY TIM package, and randomly added to the median I frame. TINY TIM models the PSF wings with good accuracy, and to avoid problems with the central peak we used a semi-empirical approach; we adapted the free parameter jitter in the TINY TIM simulation in order to reproduce the central width of the brightest observed stars. This way we got a good approximation both of the central peak and of the wings. To avoid changing the crowding conditions on the frame too much, this was done for each mag bin separately, adding no more than 2 per cent of the total number of stars each time.

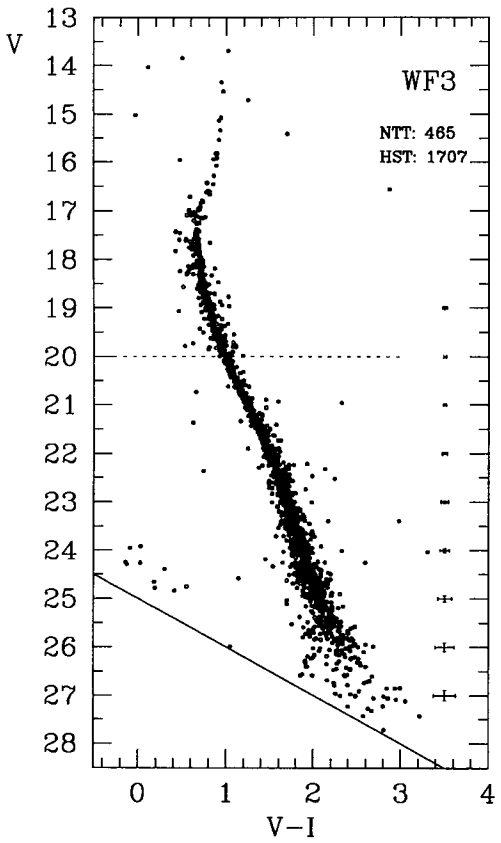

Figure 2. The V–$(V-I)$ CMD for stars within the WF3 field. Stars brighter than about $V_{555} = 20$ are saturated in the *HST* field, so we plot *HST* data below $V = 20$ and NTT data above this limit, shown by the dotted line, and indicate the number of stars in each of the two samples. The filled line denotes our search limit. Note the WD sequence at $V_{555}-I_{814} \sim 0$, and some probable binary stars on the upper right of the MS. Error bars give the error in magnitude and colour at various mag levels: they go from $\sigma_V = 0.01$ and $\sigma_{V-I} = 0.02$ to $\sigma_v = 0.11$ and $\sigma_{V-I} = 0.13$ at $V = 20$ and 27 respectively.

© Royal Astronomical Society • Provided by the NASA Astrophysics Data System

Downloaded from https://academic.oup.com/mnras/article/286/4/1012/978305 by guest on 21 August 2022

1997MNRAS.286.1012F

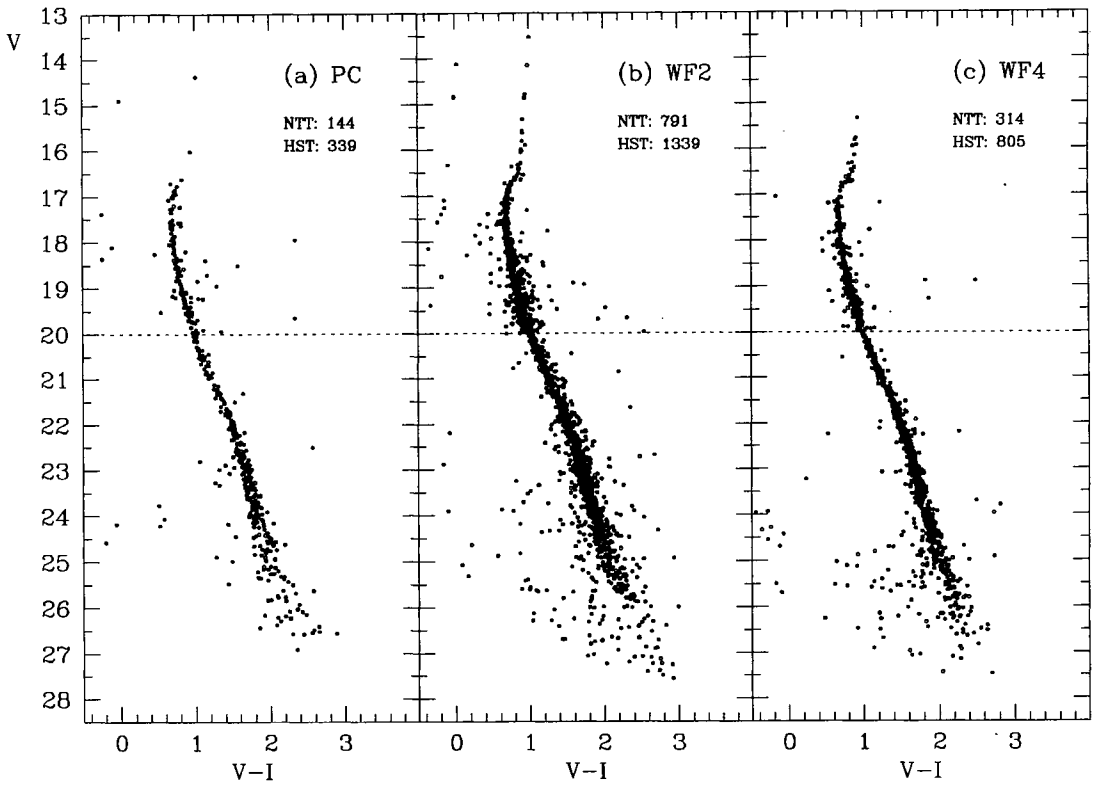

Figure 3. As in Fig. 2: V versus $V-I$ CMDs combining *HST* and NTT data for the PC (a) and the portions of the WF2 (b) and WF4 (c) analysed. Also given are the number of stars coming respectively from the NTT and *HST* samples in each camera.

Table 1. Luminosity function for WF3 in the I band in 0.5 mag bins: N is the actual number of stars found, γ^{-1} our completeness degree in each bin and NC the number of stars corrected for incompleteness.

mag interval	N	γ^{-1}	NC
18.50 - 19.00	79	0.95	83
19.00 - 19.50	142	0.94	151
19.50 - 20.00	154	0.93	166
20.00 - 20.50	167	0.91	184
20.50 - 21.00	187	0.89	210
21.00 - 21.50	217	0.87	249
21.50 - 22.00	229	0.84	274
22.00 - 22.50	186	0.79	237
22.50 - 23.00	159	0.72	222
23.00 - 23.50	106	0.63	168
23.50 - 24.00	68	0.52	130
24.00 - 24.50	34	0.40	86
24.50 - 25.00	15	0.25	60

The reduction was then repeated, starting from peak detection. We considered as being successfully recovered (N_{rec}) only those stars with output position and magnitudes in good agreement with the simulated ones, i.e. with Δ pos <2 pixel, and Δ mag <0.3. The ratio of the number of recovered stars N_{rec} to the number of simulated ones (N_{sim}) has been adopted as the completeness factor γ^{-1}. This process was repeated three times for each bin for $I \lesssim 23.5$ and six times at fainter magnitudes, and the results have been averaged. The completeness factors for WF3 are shown in Fig. 4, together with results for WF2, WF4 and PC. The error ($\sigma_{\gamma^{-1}}$) on the incompleteness factor has been estimated from the rms of multiple measures in the same bin of magnitude, and is typically $\lesssim 2$ per cent; it is about 4 per cent for WF2 and WF4, while for the PC we did only one experiment per bin.

A comparison of the completeness curves for the four fields shows that loss of stars is almost always a consequence of crowding: in fact only the most external part of WF4, which is the farthest from the cluster centre, shows a behaviour remarkably different from the other regions. In the following we will discard conservatively all mag bins where completeness is lower than 50 per cent.

3 THE LUMINOSITY FUNCTION

3.1 The luminosity function for stars within the WF3 field

To construct the LF, the following procedure was adopted. The CMD was divided into bins of magnitude (0.5 mag wide), then for each bin the mode of the colour distribution of MS stars was determined, and all stars falling within $\pm 5\sigma_{V-I}$ from the ridge line were counted.

The I-band LF for the WF3 field is presented in Table 1 and in Fig. 5, both before and after the correction for incompleteness. The uncertainty assigned to each bin is the combination of Poisson noise and the uncertainty in the correction factor. As already mentioned, in the following discussion we consider only those stars fainter than $I = 19$, and in bins the completeness factors of which are larger than 50 per cent (in practice $I<24$).

© Royal Astronomical Society • Provided by the NASA Astrophysics Data System

Downloaded from https://academic.oup.com/mnras/article/286/4/1012/978305 by guest on 21 August 2022

1997MNRAS.286.1012F

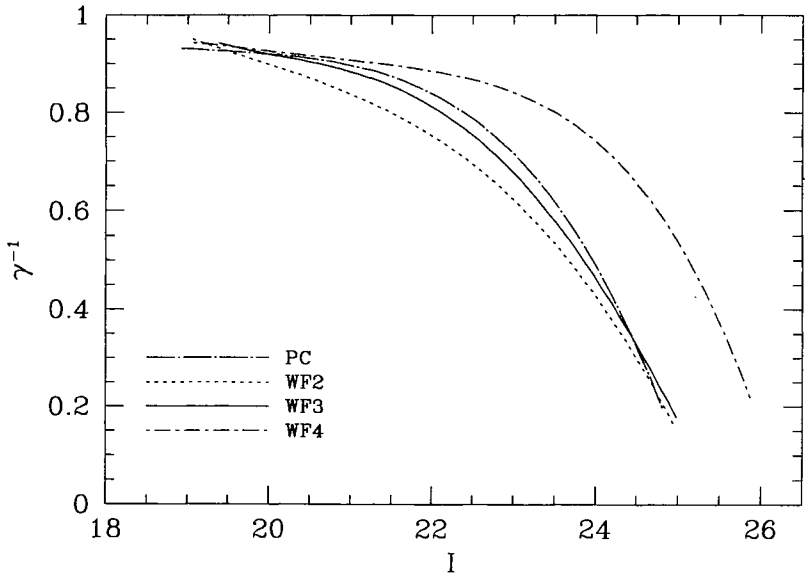

Figure 4. Completeness function for the four WFPC2 chips at various I magnitude levels, resulting from multiple experiments. Long-dash–dot line: PC; dotted line: WF2; filled line: WF3; dash–dot line: WF4.

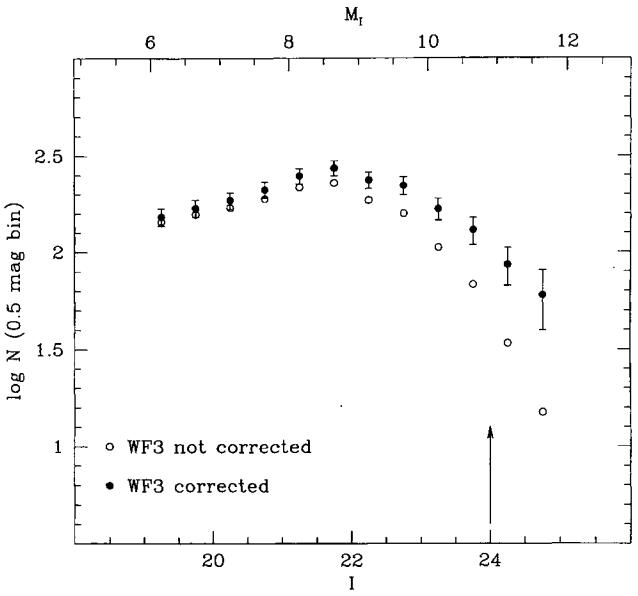

Figure 5. LF for NGC 6752, WF3, measured in 0.5 bins. Open circles: before incompleteness correction; filled circles: after correction. Error bars come from counting statistics and errors on completeness correction. The arrow indicates the 50 per cent completeness limit. The upper x-axis gives the corresponding M_I.

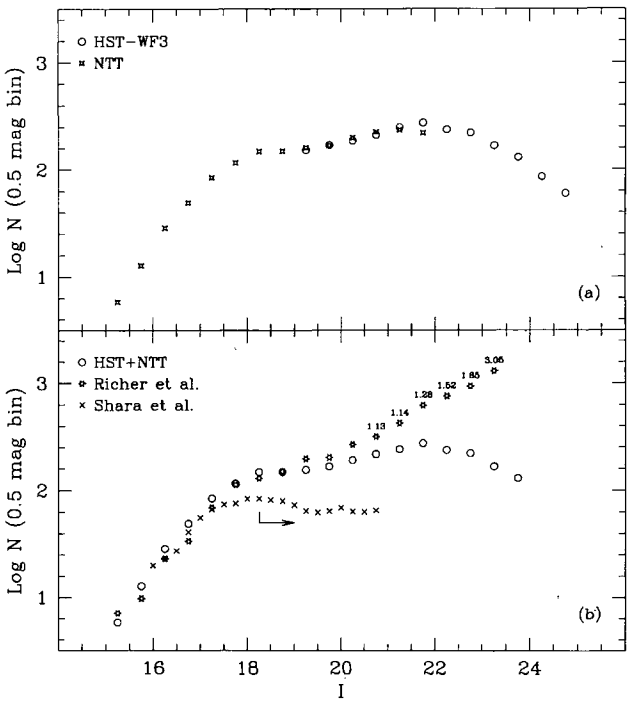

Figure 6. (a) Comparison of the LFs for NTT (stars) and WF3 data: they are very similar in the range of magnitudes in common. (b) Comparison between our LF or WF3 (open circles), complemented for $I<19$ by NTT data, and the older ground-based one determined by Richer et al. (1991, open stars). The 2 LFs have been shifted so as to best reproduce the bright LF. Also shown is the LF measured in the central part of NGC 6752 by Shara et al. (1995, crosses), shifted to reproduce their fig. 8a. All three LFs have been corrected for incompleteness. In the ground-based LF we have labelled points where the correction is more than about 10 per cent (taken from their table 3). A small arrow indicates where the Shara et al. counts begin to be corrected for incompleteness.

Conversion to absolute magnitudes was done using the distance modulus $(m\text{-}M)_0 = 13.05 \pm 0.1$ just determined for NGC 6752 with the WD method using the same *HST* observations (Renzini et al. 1996), and a reddening $E(B-V) = 0.04$ (Penny & Dickens 1986) together with $E(V-I) = 1.36\,E(B-V)$ (Taylor 1986).

The LF in NGC 6752 follows the typical pattern also seen in other globular cluster LFs obtained from *HST* data (see

© Royal Astronomical Society • Provided by the NASA Astrophysics Data System

Downloaded from https://academic.oup.com/mnras/article/286/4/1012/978305 by guest on 21 August 2022

1997MNRAS.286.1012F

references in Section 1), i.e. an increase to a rather shallow maximum followed by a steady decrease towards fainter magnitudes. As already noted by others (e.g. De Marchi & Paresce 1995a,b; Cool et al. 1996), this last trend is the opposite of that shown by the deep ground-based LFs of Richer et al. (1991).

3.2 Comparison with other LFs

Fig. 6(a) shows the LFs derived for the *HST*–WF3 data and from the NTT ones (obtained on the whole field and normalized to the *HST* data scaling with the areas). Fig. 6(b) shows the LF for the WF3 field obtained by combining WF3 and NTT data for $I<21.5$; above this magnitude the completeness correction for the NTT data is better than $\sim$60 per cent. As already noted for other clusters, a change of slope is present in the bright part, resulting in a plateau around $I\simeq19$; this is not an artefact of the combination of the two samples, since the two LFs are very similar in this range of magnitudes (see Fig. 6a). Also plotted in Fig. 6(b) is the LF by Richer et al. (1991) from ground-based observations referring to radial distances from 6 to 10 arcmin from the cluster centre, and the Shara et al. (1995) LF from *HST* data obtained with PC1 through the F785LP filter. Shara et al.'s FL refers to the innermost $\sim$15 arsec of the cluster. For comparison, we reiterate that the WF3 field extends from $\sim$2 to $\sim$3.2 arcmin from the cluster centre (see Fig. 1).

Our combined LF apppears to be intermediate in behaviour between the Richer et al. LF for the outer regions, and the Shara et al. LF for the central regions. Part of the difference between our LF and that of Richer et al. may come from these authors having possibly overestimated the correction factor for incompleteness. The opposite problem may affect the Share et al. LF, given the poorer performance of WFPC1 compared to WFPC2. However, it is likely that at least some of these differences are the result of mass segregation within the cluster, with faint, low-mass stars settling in a broader distribution as compared with more massive stars, hence leaving the central regions of the cluster depleted of faint stars. Qualitatively, the three LFs shown in Fig. 6 differ from each other as expected, given the different distance from the cluster centre. Shara et al. also interpreted in terms of mass segregation the different behaviour of their central LF as compared with the peripheral LF of Richer et al. (1991).

Finally, Fig. 7 shows the LFs of the globular clusters studied up-to-date using the *HST*: namely, those of 47 Tuc (De Marchi & Paresce, 1995b), M15 (De Marchi & Paresce, 1995a), ω Cen (Elson et al. 1995), M3 (Marconi et al. 1997) and NGC 6397 (Paresce et al. 1995; see also Cool et al. 1996). In all cases, distance moduli and reddening values were taken from the quoted papers.

In order to allow for a meaningful comparison, all LFs were normalized in two different ways: (1) by matching the numbers of stars (corrected for incompleteness) within the magnitude range $5.9\lesssim M_I\lesssim6.9$, where all the LFs have a high degree of completeness and stellar evolution effects are negligible (Fig. 7a); and (2) by matching the LF maxima (Fig. 7b).

In both representations, our LF of NGC 6752 appears much flatter than the others below the normalization point, with fewer faint stars (consistent with a mass segregation effect). The WF3 field in NGC 6752 is indeed much closer to the centre – in terms of fraction of the cluster half-light radius – than any of the *HST* fields used in the other clusters in Fig. 7. The NGC 6752–WF3 LF refers indeed to a region $\sim$1.3 half-light radii from the centre, while for all other clusters the LFs refer to regions $\sim$2 to $\sim$4 half-light radii from the centre. Actually, one can easily show that the slope

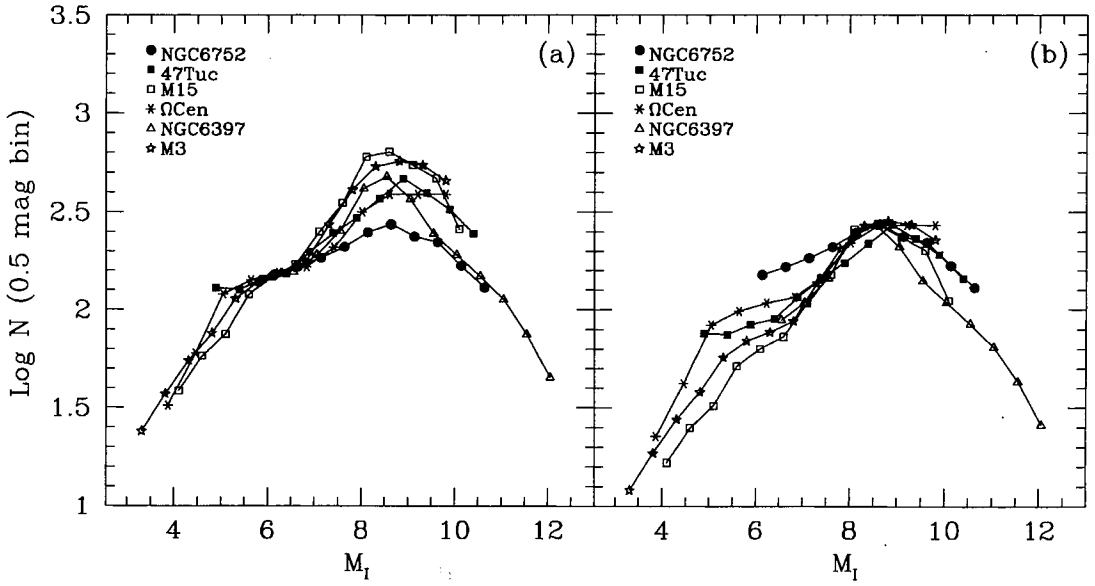

Figure 7. Comparison of the NGC 6752 LF for WF3 (filled dots) with the LFs of 47 Tuc, M15, ω Cen, M3 and NGC 6397, also obtained from *HST* data. All the LFs are corrected for incompleteness and normalized: (a) using the number of stars falling between $M_I=5.9$ and $M_I=6.9$, or (b) using the bin where the LF is at maximum. Only magnitude bins in which the completeness correction is more than about 50 per cent have been considered.

© Royal Astronomical Society • Provided by the NASA Astrophysics Data System

Downloaded from https://academic.oup.com/mnras/article/286/4/1012/978305 by guest on 21 August 2022

1997MNRAS.286.1012F

of the LF of these clusters – as measured by the LF difference between the maximum and the normalization point – correlates fairly well with the distance from the centre, measured in units of the half-light radius (Fusi Pecci et al., in preparation).

Other interpretations can easily be eliminated. For example, metallicity cannot be the cause of the difference, because NGC 6752 and M3 have nearly the same metallicity, yet quite different LFs. Seemingly, one can eliminate errors in the completeness corrections, since such errors should be of ~ 50 per cent at the LF maximum, while we estimate the corrections to be accurate within ~ 2 per cent.

3.3 The LF for the WF2, WF4, and PC fields

The presence of mass segregation effects can be further tested on our NGC 6752 data alone, as they cover a non-negligible range of distances from the cluster centre. Indeed, NGC 6752 is a very concentrated, post-core-collapse cluster, and even the small field of view of the *HST* could sample regions in different dynamical situations.

Table 2 gives results for the three LFs, and Fig. 8 shows the four LFs obtained from the single chips, corrected for incompleteness and normalized at maximum. A slight trend is visible in the sense of a varying LF moving from WF4, the more external chip, to WF2 closer to the centre, but it is too small to conclusively state that a radial gradient in the ratio of bright to faint stars can be seen. The effect is more evident when dividing the whole sample into two subsamples at different distances from the cluster centre: respectively, closer than 150 arcsec and between 150 and 300 arcsec. The two subsamples, corrected for completeness, have about the same number of stars (2133 and 2412, respectively). Fig. 9 shows the two LFs, also normalized for comparison between $I = 19$ and $I = 20$. The shapes of the two LFs look noticeably different, especially for $M_I > 8$, and the difference goes in the direction of a flatter LF for the inner sample. The Kolmogorov–Smirnov test indicates that the two LFs (in the interval $I = 18$–24) are different at the 99.78 per cent level, or $\sim 5\sigma$ significance. In Fig. 10 the cumulative distributions for both discussed samples are presented as functions of the I magnitude. We conclude that there is an appreciable difference between the two LFs, as expected from mass segregation effects.

4 THE MASS FUNCTION: COMPARISON WITH THEORETICAL MODELS

The translation of the LF into the MF is seriously affected by the uncertainties in the M–L relation. No empirical M–L relation can be safely applied to metal-poor GCs, since existing ones (e.g. the M–L relations by Kroupa, Tout & Gilmore 1993) are all derived for the solar neighbourhood, hence for near-solar metallicity. In this section we compare the cluster MFs as obtained using several different theoretical M–L relations, thus gauging their effect on the derived MFs. Since NGC 6752 has metallicity [Fe/H] $\simeq -1.5$ ($Z \simeq 6 \times 10^{-4}$), the following M–L relations have been used:

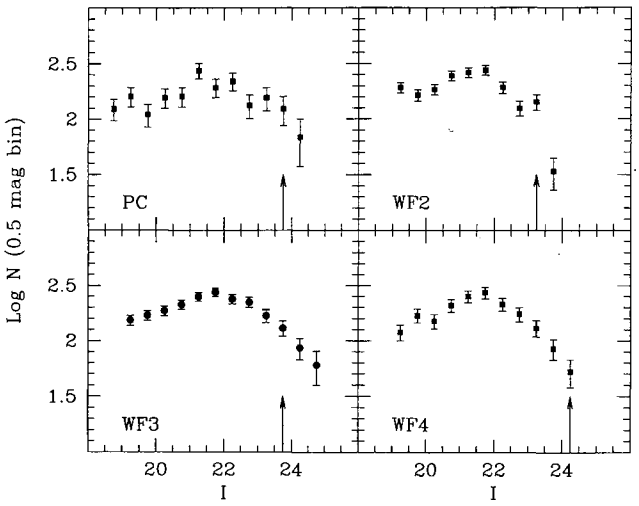

Figure 8. LFs of all the four WFC2 chips (or portions thereof) analysed, and normalized to WF3 in the bin of maximum. Note that the LF for the PC is strongly affected by small numbers oscillations. Error bars represent counting plus completeness errors, and the arrows indicate the limits for 50 per cent completeness of the samples.

Table 2. Luminosity function for the PC, WF2 and WF4 in the I band in 0.5 mag bins. Labels are as in Table 1.

I	PC			WF2			WF4		
mag interval	N	γ^{-1}	NC	N	γ^{-1}	NC	N	γ^{-1}	NC
18.50 - 19.00	25	0.93	27	68	0.95	71	12	0.95	13
19.00 - 19.50	32	0.93	35	145	0.94	154	49	0.94	52
19.50 - 20.00	22	0.92	24	120	0.91	132	69	0.93	74
20.00 - 20.50	31	0.91	34	131	0.88	148	61	0.92	66
20.50 - 21.00	32	0.90	35	168	0.85	197	83	0.91	91
21.00 - 21.50	53	0.89	60	172	0.82	210	99	0.90	110
21.50 - 22.00	36	0.86	42	171	0.78	220	106	0.89	119
22.00 - 22.50	39	0.82	48	112	0.73	154	82	0.88	93
22.50 - 23.00	22	0.75	29	66	0.66	100	65	0.86	76
23.00 - 23.50	23	0.67	34	66	0.58	114	47	0.82	57
23.50 - 24.00	15	0.56	37	13	0.48	27	29	0.77	37
24.00 - 24.50	6	0.41	15	13	0.37	36	16	0.70	23
24.50 - 25.00	1	0.22	4	9	0.23	40	4	0.60	7

© Royal Astronomical Society • Provided by the NASA Astrophysics Data System

Downloaded from https://academic.oup.com/mnras/article/286/4/1012/978305 by guest on 21 August 2022

1997MNRAS.286.1012F

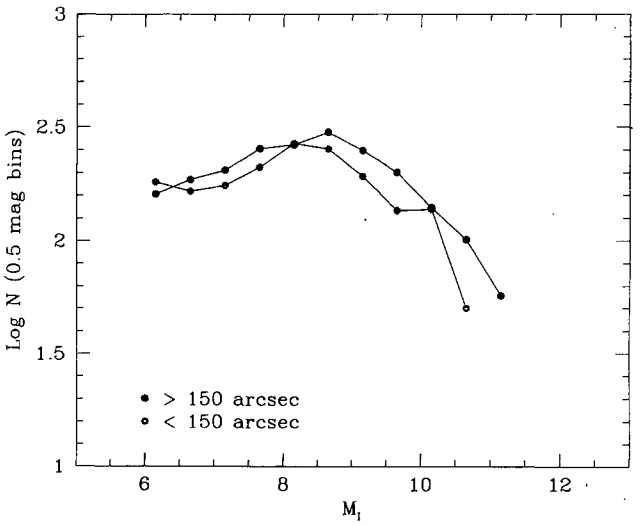

Figure 9. Radial trend of the LF, measured in two different regions, nearer of farther than 150 arcsec, whose effective distances from the centre are respectively of 2 (or 1.1 r_h), and 3.1 arcmin (or 1.6 r_h). The two LFs have been normalized to the one for WF3 in the two first bins, as has been done for all other GC LFs.

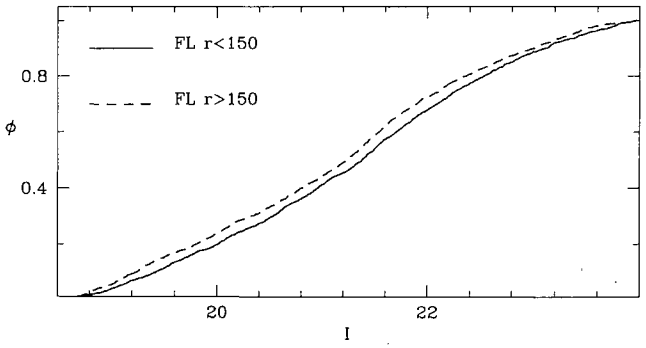

Figure 10. Cumulative distribution for the two subsamples (nearer and farther than 150 arsec from the cluster centre).

(a) Brewer et al. (1993): their M–L relation is a modification of the Richer & Fahlman (1989) semi-empirical M–L relation, derived from local metal-poor stars and subdwarfs (Rodgers & Eggen 1974) and the models of D'Antona (1987) for ($Z = 10^{-3}$).

(b) D'Antona & Mazzitelli (1996): these models employ the Canuto & Mazzitelli (1991, 1992) treatment of convection, and new opacities (Alexander & Ferguson 1994). We chose the two sequences with $Y = 0.23$, and $Z = 10^{-3}$ and 10^{-4}. The first choice seems to be more appropriate for NGC 6752, since their models do not include an enhancement of the α elements.

(c) Alexander et al. (1997): these models make use of the latest updates in input physics and Brocato et al. (1996) have successfully applied them to reproduce the MS of NGC 6397 observed with *HST* by Cool et al. (1996). We use the sequences with $Z = 1 \times 10^{-3}$, and $Z = 6 \times 10^{-4}$.

For cases (b) and (c) the sequences for an age of 10 Gyr were used, but choosing the 20 Gyr ones would not result in any appreciable difference, as we compare sections of the LF that are unaffected by stellar evolutionary effects. [Note that the age of NGC 6752 is ~15 Gyr (Renzini et al. 1996).] The CMDs and the M–L relations for the five cases are shown in Fig. 11.

These five M–L relations have been applied to the WF3 data, taking into account the completeness corrections, thus deriving mass values for each star in the sample. The corresponding mass range goes from ~0.65 down to ~0.12 $M_\odot$. Stars were then counted in bins of 0.05 $M_\odot$ and the results are shown in Fig. 12 for all five cases. The error bars come only from counting statistics in each bin and do not include any 'theoretical error' from the M–L transformation.

The MFs derived from the different M–L relations are quite similar to each other, given the associated errors, the only exception being the MF derived from the Brewer et al. (1993) M–L relation. This latter LF reaches a peak at ~0.17 $M_\odot$, then declines. The other four MFs do not show any indication of reaching a maximum, but instead keep growing towards lower masses.

A peak in the MF was also found in M15 (De Marchi & Paresce 1995a), 47 Tuc (De Marchi & Paresce 1995a) and NGC 6397 (Paresce et al. 1995), in all cases using the Brewer et al. (1993) M–L relation. No peak was found by Cool et al. (1996) in the case of NGC 6397 using the D'Antona & Mazzitelli (1996) or the Alexander et al. (1997) M–L relations, or by Elson et al. (1995) for ω Cen, where both the Brewer et al. (1993) and a synthetic M–L relation were used.

The origin of the different MF obtained when using the Brewer et al. relation can easily be traced to the different behaviour of the M–L relation shown in Fig. 11. This illustrates once more the crucial role of the M–L relation when trying to construct MFs for low-mass stars, which in fact depends more on the adopted M–L relation than on the details of the LF.

With this proviso, the MFs shown in Fig. 12 (other than that from the Brewer et al. relation) can be fitted in the interval 0.25–0.55 $M_\odot$ (i.e. to about the maximum in the LF), without taking into account any correction for segregation effects, by a power law with index $x = 1.33$ (the Salpeter slope being $x = 1.35$). As is apparent from Fig. 12, the slope of the MF declines for lower masses: in the range 0.3–0.15 $M_\odot$ we obtain $x = 0.90$. No strong inferences can be drawn from this value, since it comes from the mass interval in which the M–L relations have lower accuracy, and where our sample is less complete. Given this slope, however, it appears unlikely that a significant fraction of the total cluster mass is due to very low-mass stars (or brown dwarfs, if we presume to extrapolate the MF into that regime).

4.1 The value of M_I^{max}

Recently von Hippel et al. (1996) have pointed out that GC LFs observed with the *HST* may be consistent with a universal IMF, in spite of a weak dependence of M_I^{max} (the absolute I magnitude of the maximum in the LF) on the cluster [Fe/H]. These dissimilar values of M_I^{max} would nonetheless be consistent with a single value of mass at LF maximum (~0.25 $M_\odot$).

We have repeated the comparison using the published GC LFs, our own for NGC 6752, and the one for M3 (Mar-

© Royal Astronomical Society • Provided by the NASA Astrophysics Data System

Downloaded from https://academic.oup.com/mnras/article/286/4/1012/978305 by guest on 21 August 2022

1997MNRAS.286.1012F

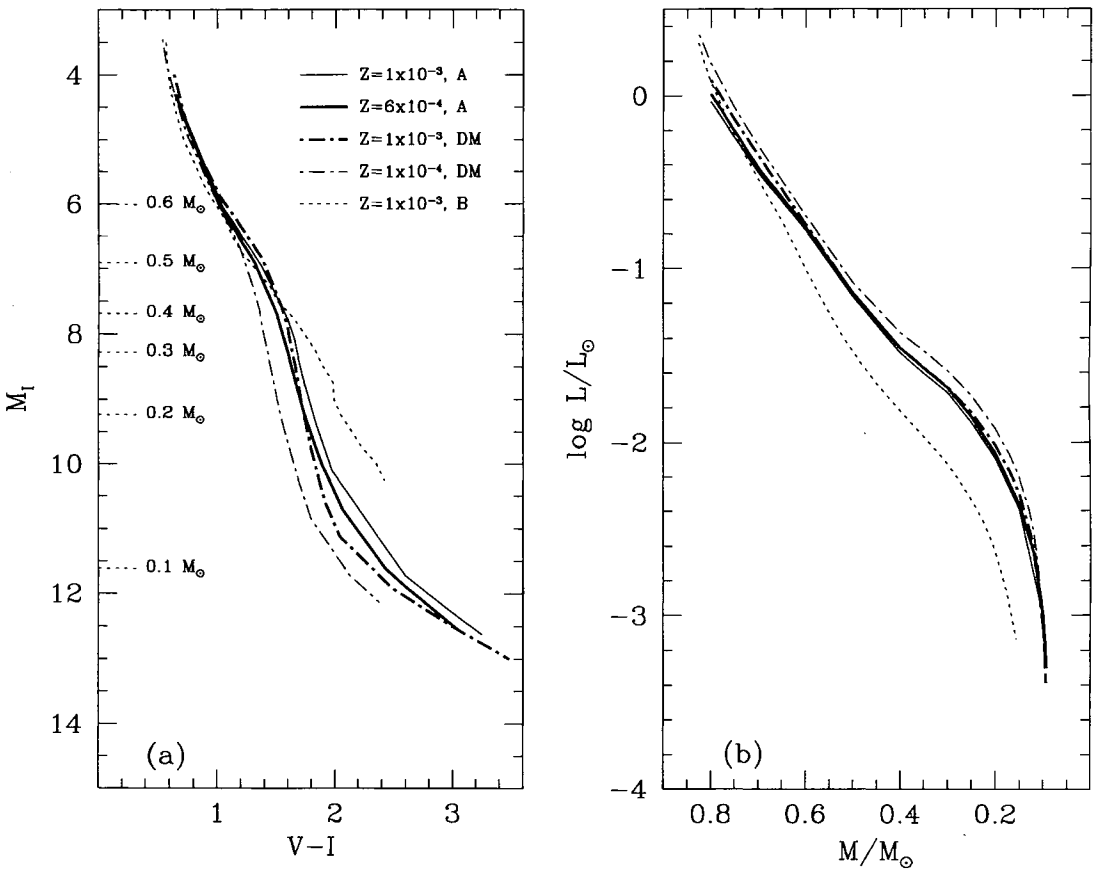

Figure 11. (a) CMD in M_I versus $(V-I)$ for the five ML relations used (A = Alexander et al. 1996; B = Brewer et al. 1993; DM = D'Antona & Mazzitelli 1996). Also indicated are some masses, computed for the A, $Z = 6 \times 10^{-4}$ model. (b) The five M–L relations, indicated in the same way.

coni et al. 1996), adopting a uniform distance scale for the clusters, rather than adopting the distance moduli given by Marconi et al. This was done to check whether the dependence of M_I^{max} on [Fe/H] may have been introduced by the assumed relation between M_V^{HB} (the magnitude level of the horizontal branch) and [Fe/H], used to derive the GC distance moduli.

We have chosen values of V^{HB} and $E(B-V)$ from Sarajedini (1994) and Peterson (1993), and metallicities from Carretta & Gratton (1997). The relation we use is $M_V^{HB} = 0.17[Fe/H] + 0.82$ (Lee, Demarque & Zinn 1994), and the results are shown in Table 3 and Fig. 13, together with the M_I magnitude for three values of the stellar mass as a function of metallicity (models from Alexander et al. 1997).

The values of M_I^{max} indicate a mass ~ 0.25 $M_\odot$ for the maximum of the LF, for all GCs irrespective of their metallicity, as already noted by von Hippel et al. (1996). As is evident from a comparison of Figs 5 and 12 (the luminosity and mass functions), a maximum in the FL does not imply a maximum in the MF.

5 SUMMARY

We have observed NGC 6752 with the WFPC2 on board the *HST*, covering a distance from ~ 1 to ~ 4 arcmin from the cluster centre, deriving a deep CMD in V and I, reaching down to $V \lesssim 27$, and a luminosity function that is robust down to $I \lesssim 24$. Effects of mass segregation within the cluster can be seen when comparing our LF to the Richer et al. (1991) and Shara et al. (1995) LFs that cover, respectively, outer and inner regions of the cluster. A radial trend in the LF is also apparent in our own data, though they span a much smaller range in distance from the centre.

The present LF of NGC 6752 reaches a maximum at $M_I^{max} = 8.6$, then declines as most other LFs obtaind from *HST* data. This value is consistent with a weak dependence of M_I^{max} on metallicity.

We have derived the cluster mass function from various M–L relations, for a total of five combinations of models/metallicity. In only one of these combinations is a maximum reached in the MF, at ~ 0.2 $M_\odot$, while in all other combinations the MF appears to increase all the way to the minimum mass reached by the photometry (~ 0.12 $M_\odot$). These results are consistent with previous result for other clusters, when the same M–L relations are used.

It is finally emphasized that an observational check of the theoretical M–L relation is required to put the derived mass functions on firmer ground, and this must be so for the various metallicities spanned by globular clusters (i.e from $\sim 1/100$ solar to over the solar metallicity).

© Royal Astronomical Society • Provided by the NASA Astrophysics Data System

Downloaded from https://academic.oup.com/mnras/article/286/4/1012/978305 by guest on 21 August 2022

1997MNRAS.286.1012F

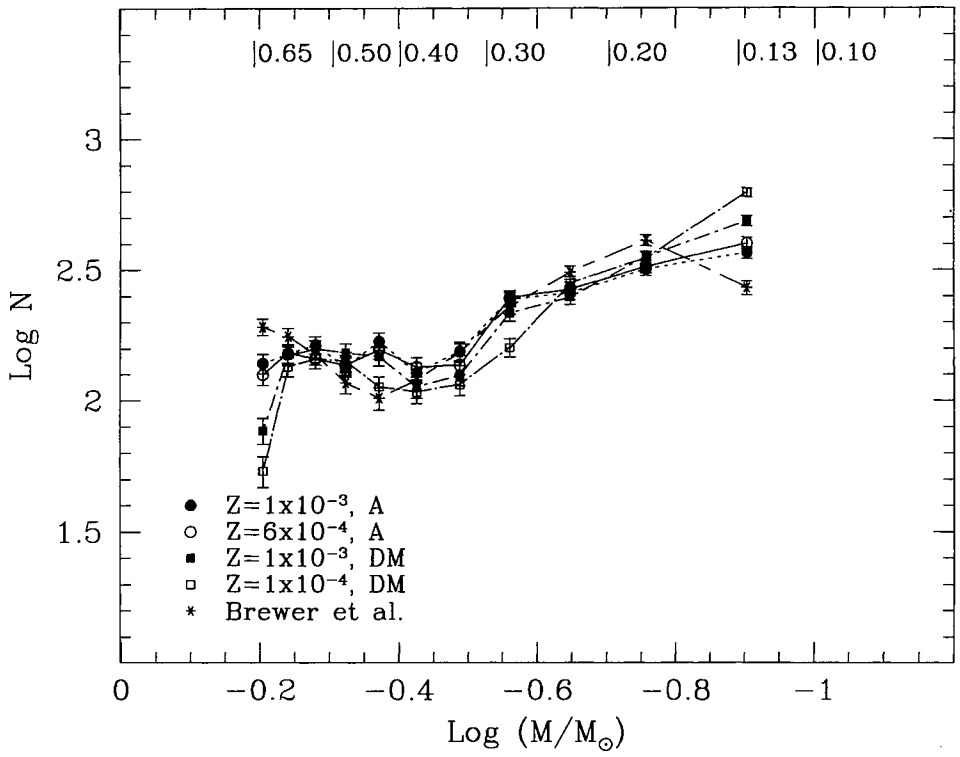

Figure 12. Mass function for the WF3 FL, as obtained from different M–L relations, indicated in the figure. The corresponding mass values are given as labels. Error bars come from counting statistics.

Table 3. Literature data and derived M_I^{max} for the 6 GCs.

GC	V(HB)	E(B−V)	[Fe/H]	M_V^{RR}	$(m-M)_I$	I_{max}	M_I^{max}
47Tuc	14.06	0.04	−0.70	0.70	13.30	22.25	8.95
ωCen	14.52	0.11	−1.36	0.59	13.77	22.79	8.93
M3	15.66	0.00	−1.34	0.59	15.07	23.75	8.68
N6752	13.75	0.04	−1.42	0.58	13.11	21.75	8.62
N6397	12.90	0.18	−1.82	0.51	12.12	20.74	8.62
M15	15.86	0.10	−2.12	0.45	15.25	23.85	8.60

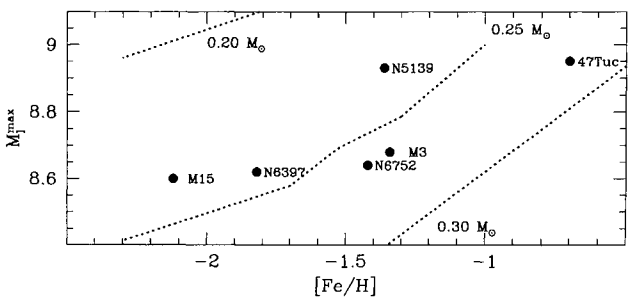

Figure 13. Value of M_I^{max} for GC of different [Fe/H]. Also shown are the models by Alexander et al. (1997) for 0.20, 0.25, 0.30 $M_\odot$, at varying Z.

ACKNOWLEDGMENTS

It is our pleasure to thank S. Cassissi for sending us the tabulated theoretical M–L relations, and F. D'Antona for helpful suggestions. We very warmly thank G. Iannicola, whose expertise on ROMAFOT was invaluable for the completion of this work. Our thanks also go to the referee Dr. R. Elson, whose comments have improved our presentation.

This paper is based on observations made with the NASA/ESA *Hubble Space Telescope*.

REFERENCES

Alexander D. R., Ferguson J. W., 1994, ApJ, 437, 879
Alexander D. R., Brocato E., Cassisi S., Castellani V., Ciacio F., Degl'Innocenti S., 1997, A&A, 317, 90
Anderson J., King I. R. 1996, in Morrison H., Sarajedini A.,eds, ASP Conf. Ser. 92, Formation of the Galactic Halo ... Inside and Out. Astron. Soc. Pac., San Francisco, p. 257
Bahcall J. N., Guhathakurta P., Schneider D. P., 1990, Sci, 248, 178
Brewer J. P., Fahlman G. G., Richer H. B., Searle L., Thompson I., 1993, AJ, 105, 2158
Brocato E., Cassisi S., Castellani V., Cool A. M., King I. R., Piotto G., 1996, in Morrison H., Sarajedini A., eds, ASP Conf. Ser. 92, Formation of the Galactic Halo ... Inside and Out. Astron. Soc. Pac., San Francisco, p. 76.
Buonanno R., Iannicola G., 1988, PASP, 101, 294
Buonanno R., Buscema G., Corsi C. E., Ferraro I., Iannicola G., 1983, A&A, 126, 278
Buonanno R., Corsi C. E., Fusi Pecci F., 1989, A&A, 216, 80
Canuto V. M., Mazzitelli I., 1991, ApJ, 370, 295
Canuto V. M., Mazzitelli I., 1992, ApJ, 389, 72
Carretta E., Gratton R. G., 1997, A&AS, 121, 95
Cool A. M., Piotto G., King I. R., 1996, ApJ, 468, 655
D'Antona F., 1987, ApJ, 320, 653
D'Antona F., Mazzitelli I., 1996, ApJ, 458, 329
De Marchi G., Paresce F., 1995a, A&A, 304, 202
De Marchi G., Paresce F., 1995b, A&A, 304, 212
De Marchi G., Paresce F., 1996, ApJ, 467, 658
Elson R. A. W., Gilmore G., Santiago B. X., Casertano S., 1995, AJ, 110, 682

© Royal Astronomical Society • Provided by the NASA Astrophysics Data System

Downloaded from https://academic.oup.com/mnras/article/286/4/1012/978305 by guest on 21 August 2022

1997MNRAS.286.1012F

Ferraro F. R., Clementini G., Fusi Pecci F., Buonanno R., Alcaino G., 1980, A&AS, 84, 59
Holtzman J. A., Burrows C. J., Casertano S., Hester J. J., Trauger J. T., Watson A. M., Worthey G., 1995, PASP, 107, 1065
King I. R., Sosin C., Cool A. M., 1995, ApJ, 452, L33
Krist J., 1994, TINY TIM User's Manual Version 4.0
Kroupa P., Tout C. A., Gilmore G., 1993, MNRAS, 262, 545
Lee Y. W., Demarque P., Zinn R. J., 1994, ApJ, 423, 248
Marconi G. et al., 1997, MNRAS, submitted
Moffat A. F. J., 1969, A&A, 3, 455
Paresce F., De Marchi G., Romaniello M., 1995, ApJ, 440, 216
Penny A. J., Dickens R. J., 1986, MNRAS, 220, 845
Peterson C. J., 1993, in Djorgovski S. G., Meylan G., eds, ASP Conf. Ser., Astron. Soc. Pac., San Francisco, p. 347
Piotto G., Cool A. M., King I. R., 1996, in Morrison H., Sarajedini A., eds, ASP Conf. Ser. 92, Formation of the Galactic Halo ... Inside and Out. Astron. Soc. Pac., San Francisco, p. 277
Renzini A. et al., 1996, ApJ, 465, L23
Richer H. B., Fahlman G. G., 1989, ApJ, 339, 178
Richer H. B., Fahlman G. G., Buonanno R., Fusi Pecci F., Searle L., Thompson I. B., 1991, ApJ, 381, 147
Rodgers A. W., Eggen J., 1974, PASP, 86, 742
Rubenstein E. P., Baylin C. D., 1997, ApJ, 474, 701
Santiago B. X., Elson R. A. W., Gilmore G., 1996, MNRAS, 281, 1363
Sarajedini A., 1994, AJ, 107, 618
Shara M. M., Drissen L., Bergeron L. E., Paresce F., 1995, ApJ, 441, 617
Stetson P. B., 1987, PASP, 99, 191
Stetson P. B., 1992, User's Manual for DAOPHOT-II
Taylor B. J., 1986, ApJS, 60, 577
Trager S. C., Djorgovski S. G., King I. R., in 1993, in Djorgovski S. G., Meylan G., eds, ASP Conf. Ser., Structure and Dynamics of Globular Clusters. Astron. Soc. Pac., San Francisco, p. 347
von Hippel T., Gilmore G., Tanvir N., Robinson D., Jones D. H. P., 1996, AJ, 112, 192

Downloaded from https://academic.oup.com/mnras/article/286/4/1012/978305 by guest on 21 August 2022

© Royal Astronomical Society • Provided by the NASA Astrophysics Data System